Building and Environment 48 (2012) 195–205

Contents lists available at SciVerse ScienceDirect

Building and Environment

journal homepage: www.elsevier.com/locate/buildenv

Effect of hilly urban morphology on dispersion in the urban boundary layer

Long Sun, Anders Nottrott, Jan Kleissl*

University of California San Diego, Department of Mechanical and Aerospace Engineering, 9500 Gilman Dr, EBU2, #580, La Jolla, CA 92093-0411, USA

ARTICLE INFO

Article history:
Received 29 March 2011
Received in revised form
3 August 2011
Accepted 3 September 2011

Keywords:
Hilly terrain
Immersed boundary method
Large-eddy simulation
Urban boundary layer
Urban pollution dispersion

ABSTRACT

Air flow and dispersion in the atmospheric surface layer are strongly affected by terrain and buildings. Through Large-eddy simulation (LES) with a three-dimensional immersed boundary method (IBM) atmospheric boundary layer flow in a hilly urban area was simulated to study turbulence and dispersion properties in and above the urban canopy. Five different domains were designed to simulate flow over an infinite sequence of hills (defined by the Witch of Agnesi and having a maximum slope of 0.26), buildings on flat terrain and buildings on the Witch of Agnesi hills (hill height to building height ratios 3/2 and 9/4). Shear stress and velocity variance above the urban canopy were smaller for the small hill with buildings compared to building array on flat terrain. Shear stress increased with the hill height for hills with buildings. For hills with buildings turbulence kinetic energy (TKE) in the urban canopy increased dramatically upwind of the hillcrest and fell below the canopy level TKE for the flat urban case in the lee of the hill. Canyon ventilation at the sub-canopy level was two to three times larger for the hilly urban case compared to the flat case, but air exchange through the top of urban canyons was not greatly affected by the hill. Our study demonstrates that urban dispersion models with the ability to handle terrain and bluff obstacles in the domain are necessary to simulate important flow features and dispersion in hilly urban environments.

1. Introduction

The microclimate in urban areas created by high population and building density influences the emission and dispersion of urban air pollution, which is responsible for acute and chronic effects on human health. One of the primary challenges for modeling air pollution transport and dispersion in urban areas is complex (hilly) terrain. Three-dimensional, computational fluid dynamics (CFD) models that explicitly resolve the interaction of individual buildings with the velocity field have been proposed as a solution to this problem [1]. Tseng et al. [2] successfully used large-eddy simulation (LES) to simulate urban pollution dispersion in a realistic model of downtown Baltimore. A related study used idealized urban canopy boundaries to simulate the flow over urban-like obstacles of random height to show that contributions to the surface drag from the tallest buildings are far in excess of their proportionate frontal area [3]. Kanda et al. [4] used LES to investigate the influence of cube density on turbulent flow characteristics in and above the canopy for an array of wall mounted cubic obstacles on flat terrain. Direct numerical simulation was performed by Coceal et al. [5] to study the mean flow and turbulence statistics over groups of urban-like, cubic obstacles having similar geometry to the model of Hanna et al. [1]. Li et al. [6] simulated pollution dispersion inside a street canyon with large height to width ratio and found high pollution concentration near building walls. The air exchange rate (ACH) in the urban canyon was found to increase with decreasing urban canyon aspect ratio. The concept of ACH (see Section 3.3, Eqs. 8a,b) is borrowed from indoor ventilation engineering and describes the volumetric air exchange per unit time in an urban canyon [6,7].

None of these studies examined the flow in urban areas built-up on variable natural topography (i.e. hilly terrain), which is a characteristic of many cities and has a significant effect on atmospheric transport and dispersion in the atmospheric boundary layer (ABL). For example, many cities on the west coast of the United States, like Seattle, Portland and San Francisco, are located in hilly terrain. Previous research on atmospheric flow over hills has focused on flow over two-dimensional humps with small curvature (low hills) and uniform surface roughness (see Figure 5.4 in [8]). In a streamline coordinate system the flow accelerates at the top of a hill due to shear from the approaching wind [9]. The mean streamlines in the accelerating wind approach the hill surface, and the wind reaches maximum velocity at the hilltop. The analytical solutions of Jackson & Hunt [9] show that if the slope of the hill is 0.2, the wind speed-up at the hillcrest is about 50% [wind speed-up is defined as the ratio of the difference between the mean velocity over the hill and the upstream (undisturbed) velocity to the upstream velocity, at the

* Corresponding author. Tel.: +1 858 534 8087; fax: +1 858 534 7599.
E-mail address: jkleissl@ucsd.edu (J. Kleissl).

0360-1323/$ – see front matter © 2011 Elsevier Ltd. All rights reserved.
doi:10.1016/j.buildenv.2011.09.005

same height above the surface]. If the hill is steep enough a separation region forms downwind. Wind tunnel experiments suggest that flow separation occurs in the lee of the Witch of Agnesi hills with maximum slope of 0.26 (see Eq. (6) and Appendix A), but experiments also indicated that flow separation and reattachment were essentially intermittent [10]. Turbulent transport and dispersion are enhanced in the lee of steep hills due to strong turbulence generation in the wake, leading to terrain amplification factors for sources downwind of the hillcrest. Other hill effects include modifications to heat and mass transfer and precipitation from orographic clouds [11].

Research on the effect of explicit roughness elements on the flow over rough hills has focused on forested hills in natural settings with densely packed roughness elements that are much smaller than the hill height [12–16]. The analytical solution of Finnigan & Belcher [14] indicates that the speed-up over a forested hill is less than the speed-up over a hill with short vegetation. Wind tunnel measurements [16] and numerical simulations [15,17] have shown that large scale flow separation occurs at a smaller slope for a hill covered with a dense vegetation canopy compared to a rough hill without vegetation.

We studied atmospheric flow over hills with urban scale roughness elements, where the hill height is on the order of the roughness elements (buildings). Section 2 describes the first implementation of a three-dimensional immersed boundary method (IBM) in a LES of the atmospheric boundary layer (Section 2.1), validation of the LES (Section 2.2), and setup of the numerical simulations (Section 2.3). In Section 3 we present the results of the simulations and focus on flow parameters relevant to dispersion. Results and conclusions are presented in Sections 4 and 5 respectively.

2. Method

2.1. Numerical method

Direct numerical simulation is impractical for high Reynolds number flows due to computational cost. The Reynolds averaged Navier–Stokes (RANS) equations cannot accurately simulate three-dimensional, unsteady turbulence in flow around a bluff body [18]. In LES the dynamics of all scales larger than the filter scale are explicitly resolved (unlike RANS), while the smaller scales are parameterized with sub-grid scale models [19–23]. For these reasons, LES is the state-of-the-art for flow simulation in the urban ABL [24].

The governing equations for mass and momentum conservation are

$$\frac{\partial \overline{u_j}}{\partial x_j} = 0 \tag{1}$$

$$\frac{\partial \overline{u_i}}{\partial t} = -u_j\left[\frac{\partial \overline{u_i}}{\partial x_j} - \frac{\partial \overline{u_j}}{\partial x_i}\right] - \frac{\partial \overline{p}}{\partial x_i} + F_i + f_i - \frac{\partial \tau_{ij}^r}{\partial x_j}. \tag{2}$$

In Eqs. 1 and 2 the overbar indicates a filtered variable, u_i is the velocity vector ($i = 1,2,3$), $\overline{p} = \overline{p^*}/\rho + \tau_{kk}/3 + \overline{u_j u_j}/2$ is the filtered modified pressure, p^* is the pressure [25] and ρ is the air density. F_i is the external force consisting of a mean streamwise pressure forcing, τ_{ij}^r is the deviatoric part of the sub-grid scale (SGS) stress tensor and the convective term is written in rotational form. The flow is forced with an imposed pressure gradient in the x direction$(1/\rho)\nabla p = u_*^2/H$, where H is the height of domain and u_* is the friction velocity. In the vertical direction (z) a no-slip bottom boundary condition and stress-free upper boundary condition are imposed and derivatives are calculated on a staggered grid using a centered finite difference formula. Periodic boundary conditions are applied in the horizontal directions (x and y) and derivatives are calculated using a Fourier spectral method. The second order Adams-Bashforth scheme is applied for time advancement.

Traditionally LES of the ABL uses Cartesian or rectilinear grids and finite difference discretization. For these grid types the IBM can be applied to impose boundary conditions on non-flat surfaces [26]. Mohd-Yusof [27] introduced the feedback force to the IBM and Tseng and Ferziger [28] extended the IBM by implementing the "ghost cell" method. Tseng and Ferziger used velocity and scalars computed near the boundary of an obstacle to reconstruct a second order accurate feedback force, applied at ghost cells inside the obstacle, to enforce appropriate boundary conditions at the obstacle surface. This approach permits stable time-integration of the governing equations and results in good agreement between simulations and experimental measurements.

Choosing rectangular buildings for which the walls coincide with grid lines, simplifies the derivation of the feedback force since no interpolation between boundary and internal points is necessary. Existing LES codes that have applied the IBM to the ABL in urban areas were limited to cube-shaped buildings on a flat surface [1,2,4,5]. In contrast to urban scale models, numerical models of the atmosphere at meso-scale or larger often work in curvilinear coordinate systems (i.e. terrain following coordinates). Although hilly terrain can be represented, accurate simulation of flows over steep topography is not possible with curvilinear coordinates, which makes them generally unsuitable for building resolving simulations in urban areas [29]. Lundquist et al. [30] employed a two-dimensional IBM to represent buildings in a coupled meso-scale/LES model that used a curvilinear pressure based coordinate system. In a method limited to flow over sinusoidal hills, Wan et al. [31] used an unstructured method with LES.

Our implementation of the IBM for atmospheric LES is novel because it is generalizable to any three-dimensional boundary. The IBM force f_i is applied at internal boundary points to enforce the no-slip velocity boundary condition. f_i is derived by discretizing Eq. (2) and replacing u^{n+1} with V^{n+1} to yield

$$f_i = -\mathrm{RHS}_i + \frac{V^{n+1} - u^n}{\Delta t}, \tag{3}$$

where V^{n+1} is the velocity extrapolated from nearby grid points and RHS_i is the right-hand side of Eq. (2) (without f_i). The computational cost of calculating this force over the entire boundary is orders of magnitude smaller than the computational cost of the rest of the LES. To avoid Gibbs ringing in the computation of horizontal derivatives an interpolation scheme was applied to smooth the velocity field inside the boundary [2]

$$u_i^t(x,y) = (1-4\alpha)u_i^{t-1}(x,y) + \alpha\Big[u_i^{t-1}(x,y+\mathrm{d}y) + u_i^{t-1}(x,y-\mathrm{d}y) + u_i^{t-1}(x+\mathrm{d}x,y) + u_i^{t-1}(x-\mathrm{d}x,y)\Big] \tag{4}$$

where $\alpha = -0.125$, t is the timestep and $i = 1, 2$.

The closure of Eq. (2) requires a SGS model which parameterizes the effect of the unresolved scales on the resolved LES flow field [32,33]. The most commonly used SGS model is the Smagorinsky model [34], which relates the deviatoric part of the SGS stress tensor τ_{ij}^r to the filtered rate of strain. The SGS eddy viscosity ν_r is related to the characteristic filtered rate of strain by analogy to the mixing length hypothesis.

$$\tau_{ij}^{r} = -2\nu_r \bar{S}_{ij}$$
$$\nu_r = l_s^2|\bar{s}| = (C_s\Delta)^2|\bar{s}| \quad (5)$$

In Eq. (5) l_s is the Smagorinsky length scale, C_s is the Smagorinsky coefficient, Δ is the filter size, $\bar{S}_{ij}$ is the filtered strain rate tensor and $|\bar{s}| = \sqrt{2\bar{S}_{ij}\bar{S}_{ij}}$.

For isotropic, homogeneous turbulent flow the value of the Smagorinsky coefficient is approximately 0.17 in the inertial subrange, with the sharp spectral filter at width Δ equal to the grid size [35]. In our simulations the spectral cut-off filter had a filter size equal to the horizontal grid spacing. For anisotropic flow, C_s depends on the flow regime; C_s decreases near walls and in stably stratified conditions, and C_s is zero in laminar flow. Given the complex geometry in our simulations, advanced SGS models are required to determine C_s dynamically from the resolved scales in the simulation. The Lagrangian scale-dependent dynamic Smagorinsky model is employed in this research [36,37]. The model determines an appropriate value of the Smagorinsky coefficient locally and dynamically during the simulation without a priori tuning, resulting in more realistic near-wall dissipation characteristics and energy spectra than the original 'static' or plane-averaged Smagorinsky model [23]. For a detailed discussion of the scale-dependent dynamic Smagorinsky model the reader is referred to [23,33,37].

2.2. Validation for sinusoidal hills

The IBM implementation for surfaces aligned with the numerical grid was previously validated by [2] for flow around a single bluff body and an array of cubes, which are relevant test cases for urban simulations. We reran these cases using our model and obtained results consistent with [2].

Therefore the validation of our IBM implementation is focused on flow over sinusoidal hills and we compare our results to experimental data from a meteorological wind tunnel experiment [38] and to LES with the coordinate transformation method [31]. The experiments of [38] used a polyurethane foam model of a sinusoidal wave [$f(x,y)=a\cdot\sin(x/\lambda)$] as the lower boundary in the wind tunnel with 16 cycles of wavelength $\lambda = 607$ mm, a trough to crest height $2a = 96.5$ mm and a maximum slope of 0.5. The model was immersed in a deep turbulent boundary layer (depth 600 mm), and measurements were conducted over the 10th and 12th waves of the model so as to closely approximate flow over an infinite, two-dimensional sinusoidal surface, which is similar to the periodic boundary conditions used in our simulation. The free stream velocity was $U_o = 10$ m s^{-1}.

The computational domain in our simulation was chosen to match the height of the boundary layer in the wind tunnel experiment (Fig. 1) with $L \times W \times H = (4\pi, 2\pi, \pi + 0.249)L_z$, where the length scale $L_z = \lambda/\pi = 1.94$ m. The computational domain was divided into 96 × 16 × 97 grid points with equal grid spacing. 60,000 timesteps of $\delta t = 0.009$ s were simulated and time averages over 12,000 timesteps (=128 s) were analyzed.

Wan et al. [31] simulated a domain with a sinusoidal lower boundary similar to the one used by [38] using LES with the terrain following coordinate transform proposed by Clark [39]. The transformation $z^* = H(z - z_s)/(H - z_s)$, where z, H and z_s denote vertical position, actual elevation and surface elevation in the original coordinate system and z^* is the vertical position in the transformed system, allows a domain with a sinusoidal lower boundary to be represented on a Cartesian grid.

Fig. 2 shows a comparison of non-dimensional streamwise velocity profiles at four positions in our computational domain with data from the wind tunnel experiment and the LES with coordinate transformation. At the wave crest (Fig. 2a) the IBM simulations are in agreement with the experimental data above $z = 100$ mm, but underestimate velocity speed-up near the surface. At 1/4 wavelength downwind of the crest (Fig. 2b) the IBM simulations agree better with the experimental data than coordinate transformation method results. At the wave trough (Fig. 2c) all simulations show similar negative velocities in contrast to the positive velocities measured in the wind tunnel. Gong et al. [38] pointed out that below 50 mm a flow recirculation zone developed downwind of the wave crest, but their hot wire anemometer could not distinguish between positive and negative velocities which caused experimental error. At 1/4 wavelength downwind of the trough (Fig. 2d), the differences between all the LES models and the experimental data are small; the IBM is in close agreement with the laboratory measurements.

Normalized standard deviations of the resolved streamwise and vertical velocities over the wave crests are presented in Fig. 3. The coordinate transform method with different SGS models overestimates (σ_u/U_o) in the height range (10 mm $< z <$ 100 mm) by about 20% and 50% respectively (Fig. 3a), while our model overestimates $\frac{\sigma_u}{U_o}$ by about 25% in the same height range. The IBM simulations agree with the vertical velocity standard deviation ($\frac{\sigma_w}{U_o}$) measured during the wind tunnel experiment in the lower part of domain ($z < 100$ mm), but overestimate $\frac{\sigma_w}{U_o}$ by about 10% above 100 mm (Fig. 3b). Generally the IBM shows good agreement in the velocity field with existing data for turbulent flow over a sinusoidal bottom boundary.

These validations demonstrate that LES integrated with the three-dimensional IBM can be used to accurately simulate air flow over hills. And three-dimensional IBM allows any shape of obstacle and complex terrain to be implemented efficiently on rectilinear grids (unlike the coordinate transformation method), which is the primary advantage of the IBM approach.

2.3. Numerical experiments

Five cases were simulated with 160 × 48 × 161 grid points resolving a computational domain of 2000 m × 600 m × 1000 m in x, y and z directions. This grid resolution resulted in seven nodes inside and between buildings, a requirement to accurately simulate flow around a bluff body (as shown by [2] and [40]). The

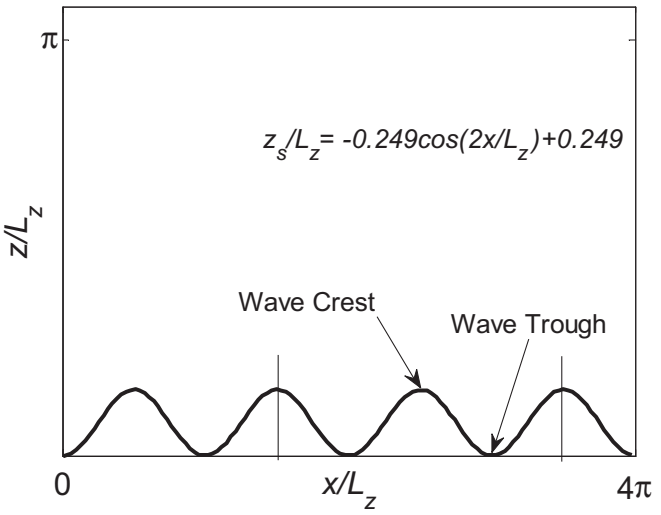

Fig. 1. Cross-section of the computational domain for the LES over two dimension sinusoidal hills. The hill surface is described by $z/L_z = 0.249\cos(2x/L_z)$.

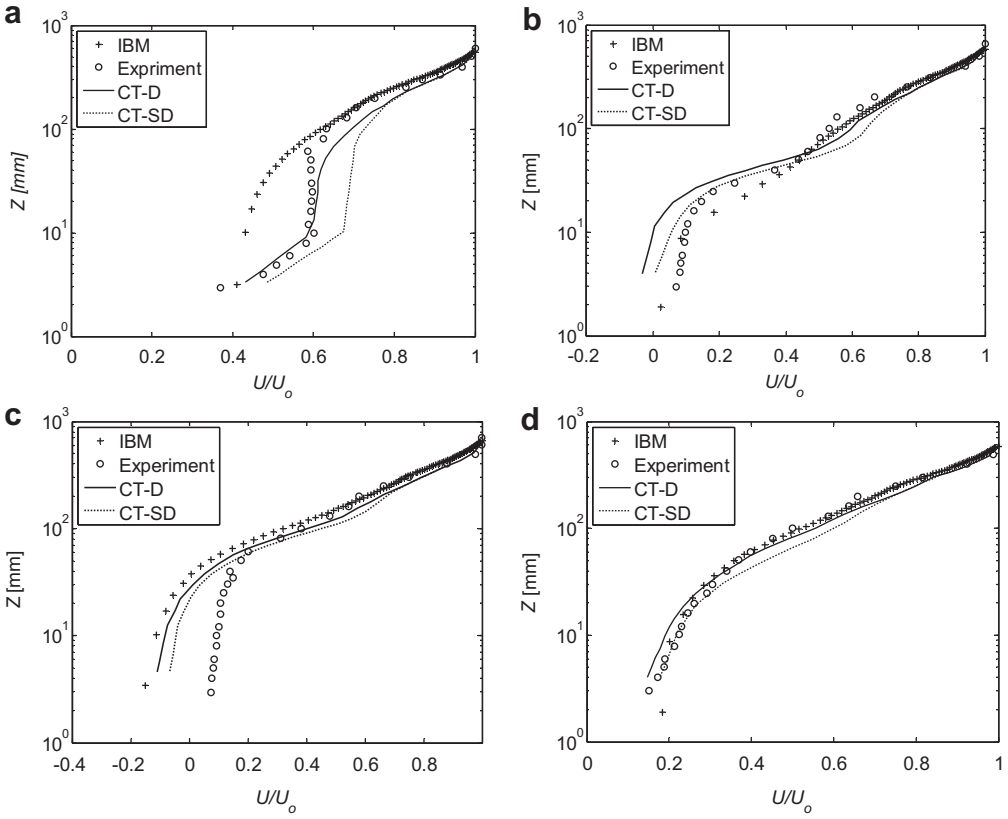

Fig. 2. Non-dimensional streamwise velocity profiles over the domain shown in Fig. 1 using the IBM with the scale-dependent dynamic SGS model (IBM). The results are averaged over the spanwise (y) direction. Measurement height above the local surface (z) is shown on the vertical axis. Results from the LES with coordinate transform using the Lagrangian dynamic and scale-dependent dynamic SGS models (CT-D and CT-SD reproduced from [31]) and wind tunnel measurements from [38] (Experiment) are shown for reference. Vertical profiles are plotted at different streamwise (x) positions: a) the wave crest; b) 1/4 wavelength downwind of the crest; c) the wave trough; d) 1/4 wavelength downwind of the trough.

computational grids and time increment were carefully selected in accordance with the guidelines of COST Action 732 [41] to ensure adequate spatial and temporal resolution of all building elements and important flow features. The simulations were initialized by imposing a log–law profile for the streamwise velocity and random values for spanwise and vertical velocities. Due to the large grid spacing the time increment for all five cases was set to be 0.0889 s and 96,000 timesteps were simulated. The results were examined for convergence to a statistical steady state and averages over the last 24,000 timesteps were used in the analysis (2134 s or at least 12 eddy turnover times based on hill height and shear stress). The flow in all simulations was neutrally stratified. The surface topography for the first case named BLDG is a 10 × 3 building array (Fig. 4a) with a building size of 100 m × 100 m × 50 m ($L \times W \times H$). The spacing between buildings is 100 m in the x and y directions. Periodic boundary conditions in the horizontal directions result in an infinite homogeneous urban surface boundary. The second and third case are flow over the Witch of Agnesi hills (an infinite sequence due to the periodic boundary condition) with maximum slope ratio $dH/dx = 0.26$ (Fig. 4b), and surface height H defined by

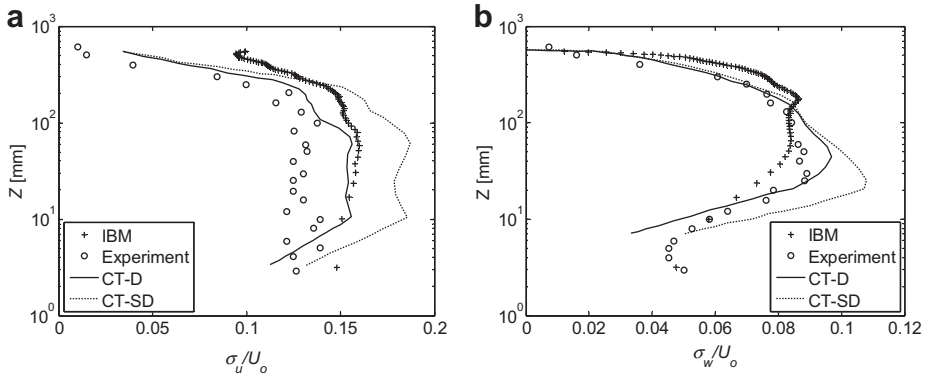

Fig. 3. Standard deviation of the resolved velocity at the wave crest normalized by the free stream velocity. The coordinate transform method with different SGS models (CT-D and CT-SD reproduced from [31]), the IBM method (IBM) and wind tunnel experiments (Experiment [38]): a) streamwise velocity; b) vertical velocity.

$$H(x) = \frac{H_{max}}{1 + \left(\frac{x}{L}\right)^2}, \quad (6)$$

with $x = 0$ located at the center of domain. The maximum hill heights H_{max} are 75 m and 112.5 m in the simulations named H75 and H113 respectively. The length scales for these two cases are H_{max} and $L = 2.5H_{max}$. The final two cases are flow over buildings arranged as in case BLDG, but placed on the hills in cases H75 and H113 (Fig. 4c; the planform arrangement of buildings is the same for domains BLDG, BH75 and BH113). These cases are named BH75 and BH113.

Generally in fluid mechanics it is desirable to show non-dimensional results, however, in our simulations there exist a variety of spatial scales, such as building height and length, hill height and half width, roughness length and boundary layer height. It is not fundamentally clear which scale could be used universally to collapse profiles. For this reason we will use dimensional length scales to present our results, unless it is clear which scale is appropriate. All heights z are taken as the height above the bottom boundary of the simulation domain, i.e. not the height above the hill surface.

3. Results

3.1. Mean velocity and velocity variances over hills

Data from wind tunnel experiments by Britter et al. [10] are compared to numerical simulations for flow over a hill without buildings (H75 and H113). In the wind tunnel experiment, the Witch of Agnesi hills were setup according to Eq. (6) with $H_{max} = 0.1$ m, $L = 0.25$ m ($H_{max}/L = 0.4$ as in the LES) and located 17.5 m downwind of the start of the wind tunnel boundary layer. Measurements of the mean velocities and rms turbulent velocities σ_u were taken at $x = -0.64, -0.25, 0, 0.25, 0.70$ m or $x/H_{max} = -6.4, -2.5, 0, 2.5, 7.0$, where $x = 0$ is located at the hillcrest in the center of the domain. The simulated case does not exactly correspond to the experiment, because periodic boundary conditions are used in the LES resulting in flow over an infinite series of hills. However, with distances between hill crests of 27 H_{max} (H75) and 18 H_{max} (H113), the downwind hillcrest is far from the reattachment point indicating that the effect of the wake generated by the upwind hill on the flow around the downwind hill was small.

The velocity fields over the hill (Fig. 5) show that flow separation begins at the hillcrest and the separation layer thickness grows to around 30% of the hill height. Reattachment occurs at 5 to 7 H_{max} (or 2 to 2.5 L) downstream of the hillcrest which is consistent with Britter et al. [10]. Since H113 has the same slope as H75, their separation regions are expected to be similar as confirmed in Fig. 5 and consistent with the wind tunnel observations.

In Fig. 6 the mean and standard deviation of the streamwise velocity at five locations along the x-axis are compared to the experimental data at three displacement distances above the hill surfaces. As expected flow speed-up is observed at the hilltop and the wake region downwind of the hill shows small wind speeds (Fig. 6a). For small displacements above the hill surface ($\delta z/H_{max} \ll 1$) the maximum velocity at the hilltop is twice the velocity in the wake, and 22–42% larger than the velocity upwind of the hill. As $\delta z/H_{max}$ increases the velocities become horizontally homogeneous and the impact of the hill diminishes. The velocities in simulation H113 agree with the experimental results, while the H75 simulation underestimates the velocities around 5–15% compared to the wind tunnel data.

Both the Britter et al. [10] experiment and our simulations confirm that the standard deviation of the streamwise velocity (σ_u)

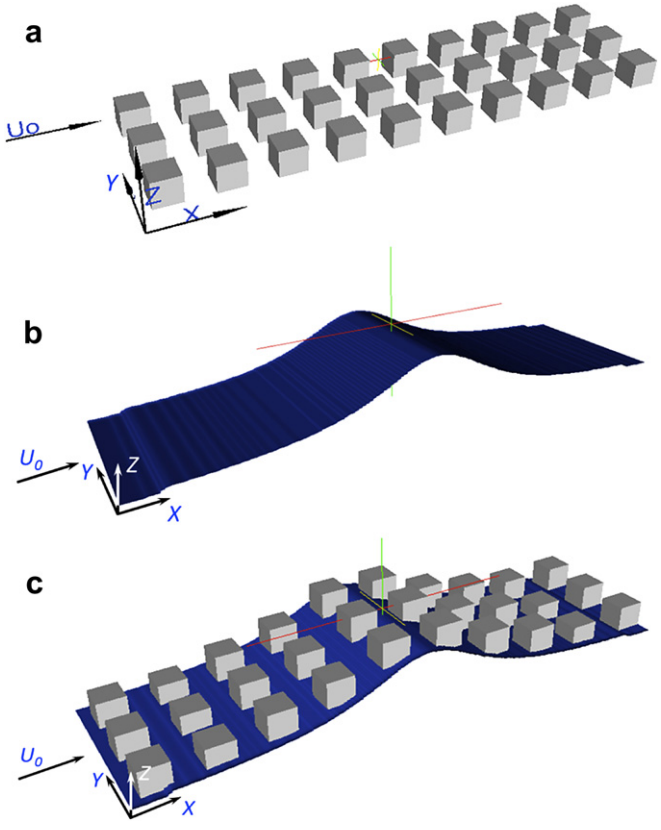

Fig. 4. Layout of the different simulation domains. a) A flat building array (BLDG); b) a hill with maximum height of 75 and 112.5 m (H75 and H113); c) buildings on a hill with H_{max} of 75 and 112.5 m (BH75 and BH113).

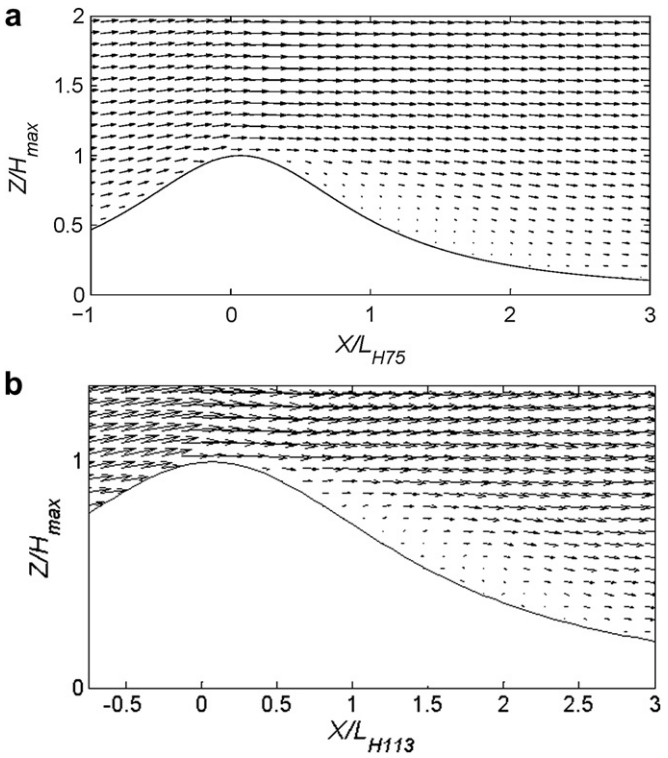

Fig. 5. Mean x–z velocity vectors near the hill surface over a) H75 and b) H113. The vertical domain extends beyond the upper limit of the figures.

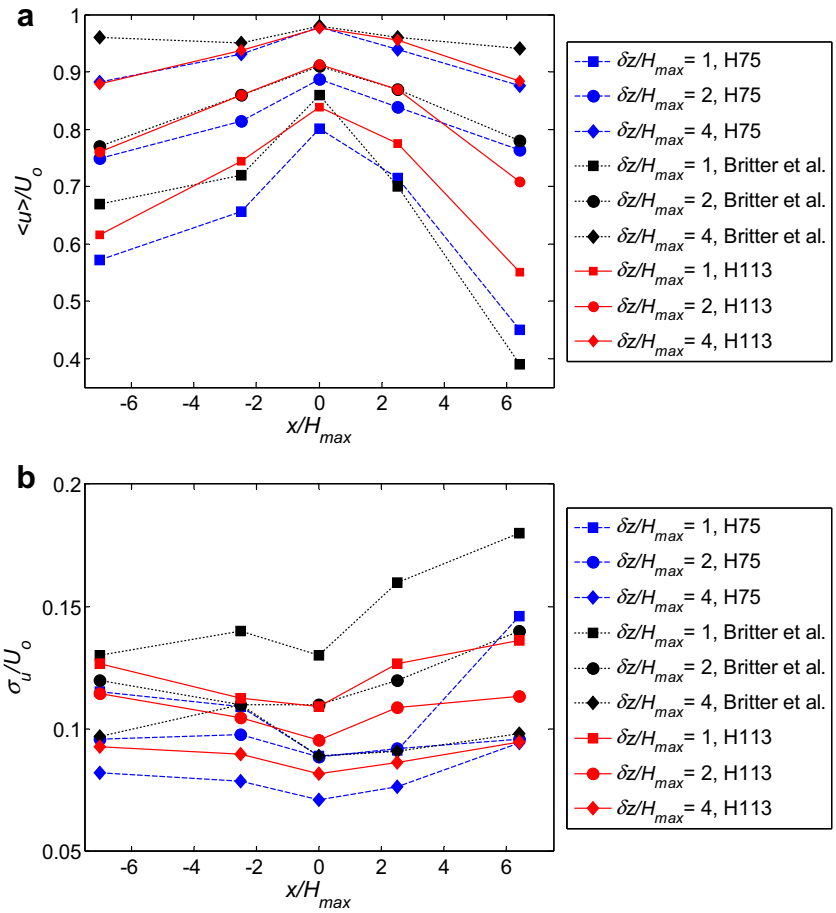

Fig. 6. Comparison of a) mean and b) standard deviation of the streamwise velocity from the experiments of [10] and LES-IBM simulations. The experimental data are normalized by the free stream velocity and the simulations are averaged over the y direction, and normalized by the velocity at $z = 4\ H_{\max}$ above the hill surface at five locations along the x-axis upwind and downwind of the hill. δz is the displacement above the hill surface and $H_{\max}$ is the hill height.

decreases near the hillcrest in the same region where speed-up of the streamwise velocity is observed (Fig. 6b). Downwind of the hillcrest a large value of σ_u is observed in both the simulations and the experiment at $\delta z/H_{\max} = 1$, near the edge of the separated shear layer for H113. This effect is strongest near the surface of the hill but persists even for $\delta z/H_{\max} = 4$. The H75 simulation underestimates σ_u by 20%–30%, and the H113 simulation underestimates by 10%–20% relative to the wind tunnel measurements. This underestimation is possibly a result of the no-slip condition in our simulations versus the rough surface (roughness height of 0.02 m) in the experiment. We find that the LES simulation of flow over the hill produces realistic velocity profiles and speed-up effects, and accurately predicts the location and size of the separation region in the lee of the hill.

3.2. Velocity profiles for all simulations

Fig. 7 shows mean streamwise velocity profiles from all five simulations measured upwind, over and downwind of the hill ($x = -800$, -400, 0, 400 and 800 m and $y = 300$ m). Note in the simulations that include buildings all vertical profiles are taken between buildings at the center of the urban canyon and extend to the ground surface level (rather than building roof level). The greatest differences between these velocity profiles occur below $z = 200$ m (in the urban canopy layer). The vertical velocity profiles in BLDG are homogeneous in x because the arrangement of roughness elements at the lower boundary of the domain is homogeneous. The velocities observed in BH113 and BH75 are generally the smallest of all five simulations due to the large amount of drag from the hill.

3.3. Air exchange rates and determinants of dispersion

The bulk quantities of average air exchange rate ($\langle \mathrm{ACH}_{\mathrm{top}} \rangle$ and $\langle \mathrm{ACH}_{\mathrm{side}} \rangle$), turbulent kinetic energy ($\langle \mathrm{TKE} \rangle_{\mathrm{total}}$) and kinetic energy ($\langle \mathrm{KE} \rangle_{\mathrm{total}}$) provide measures of the efficiency of air removal along the sides and top of urban canyons (see Fig. 8). They are defined as [7],

$$\mathrm{ACH}_{\mathrm{top}} = \frac{\int_{A_{\mathrm{top}}} w'' \mathrm{d}x\mathrm{d}y}{A_{\mathrm{top}}}, \tag{8a}$$

$$\mathrm{ACH}_{\mathrm{side}} = \frac{\int_{A_{\mathrm{side}}} v'' \mathrm{d}x\mathrm{d}z}{A_{\mathrm{top}}}, \tag{8b}$$

$$\langle \mathrm{TKE} \rangle_{\mathrm{total}} = \frac{\int_{V_{\mathrm{canyon}}} \left\langle u''^2 + v''^2 + w''^2 \right\rangle \mathrm{d}V}{V_{\mathrm{canyon}}}, \tag{8c}$$

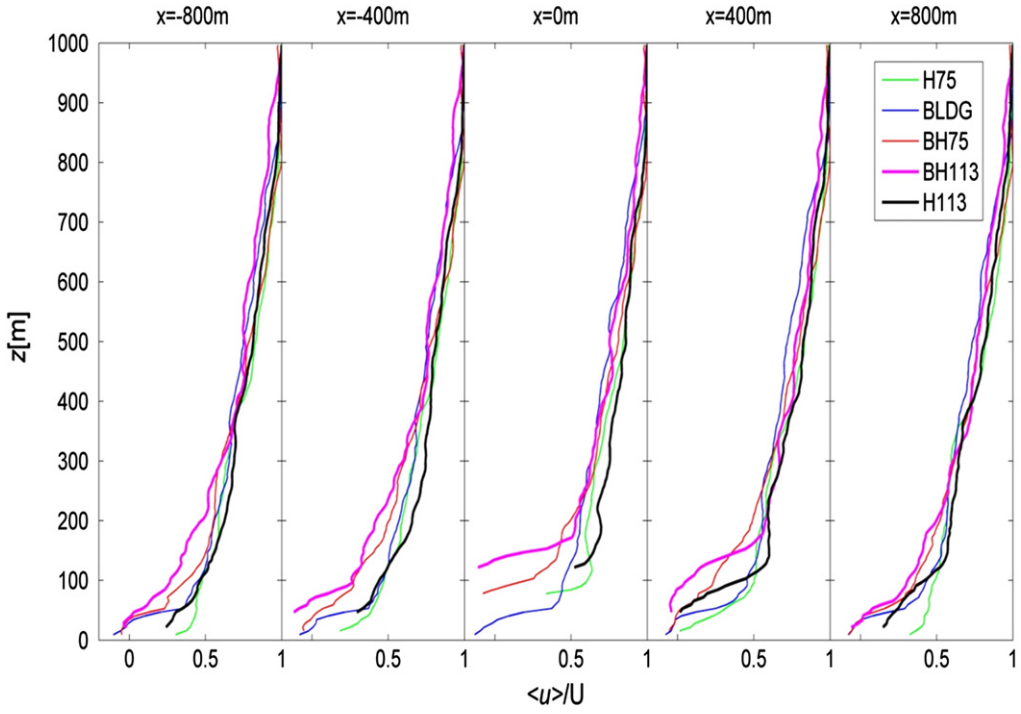

Fig. 7. Vertical profiles of mean streamwise velocity at 5 locations along the *x*-axis. Profiles are averaged over the *y* direction, averaged in time and normalized by the mean streamwise velocity at the top of the domain U_o.

$$\langle \mathrm{KE} \rangle_{\mathrm{total}} = \frac{\int_{V_{\mathrm{canyon}}} \left\langle \overline{u}^2 + \overline{v}^2 + \overline{w}^2 \right\rangle \mathrm{d}V}{V_{\mathrm{canyon}}}. \tag{8d}$$

In Eqs. 8a,b,c u'', v'' and w'' are the components of the velocity fluctuation obtained from a Reynolds decomposition of the filtered velocity (i.e. $u'' = \overline{u} - \langle \overline{u} \rangle$). A_{top} and A_{side} are the areas of the top and side of the urban canyon and V_{canyon} is the volume of the space between two buildings (Fig. 8). It is important to note that we can only examine resolved velocities in our simulation ignoring the SGS contribution.

Fig. 9 shows $<\mathrm{ACH}_{\mathrm{top}}>$, $<\mathrm{ACH}_{\mathrm{side}}>$, $<\mathrm{KE}>_{\mathrm{total}}$ and $<\mathrm{TKE}>_{\mathrm{total}}$ along the *x* direction in urban canyons as illustrated in Fig. 8. The quantity $<\mathrm{ACH}_{\mathrm{chtop}}>$ is also shown in Fig. 9c, which is similar to $<\mathrm{ACH}_{\mathrm{top}}>$ but calculated at the roof level of the urban canyon (channel) oriented parallel to the *x*-axis (i.e. $<\mathrm{ACH}_{\mathrm{chtop}}>$ is computed for a surface that has the same total area as "Top" in Fig. 8, but is shifted by a distance *W* in the *y* direction). In Fig. 9a,b and c positive air exchange rates only consider air leaving the urban canyon (see v''_+ and w''_+ in Fig. 8), while negative air exchange rates only consider air entering the urban canyon (see v''_- and w''_- in Fig. 8). Liu et al. [7] found that positive and negative air exchange rates balance each other because they studied a single closed urban canyon that was infinitely long in the spanwise direction with a periodic spanwise boundary condition, assumed incompressibility of the flow. We also observed a balance between positive and negative ACH in our simulations (Fig. 9a,b and c), which was not necessarily expected since it is possible for the sides of the canyon to have a net in flow if the top of the canyon has a net outflow. However, our observation is consistent with knowledge of recirculating eddies that are typical in cavity flows and the absence of buoyant forcing because we simulated neutral stratification.

The mean air exchange rates and kinetic energies are relatively constant along the streamwise direction for the BLDG simulation

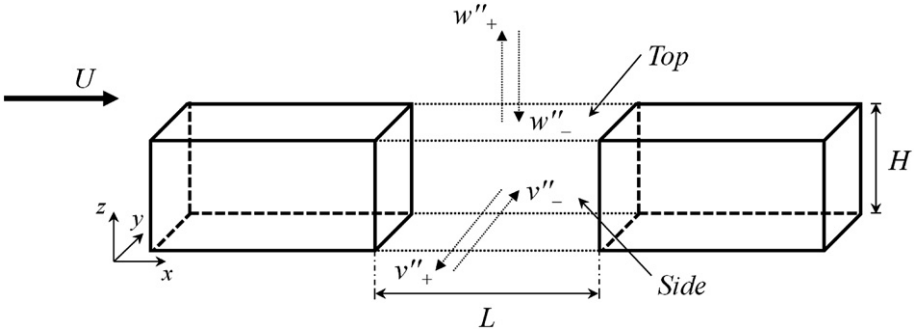

Fig. 8. A sketch of the variables used to calculate the air exchange rates between the urban canyon and the surrounding atmosphere. For buildings on the hill, the "top" and "chtop" subscripts are defined by a plane connecting two adjacent building roofs and applying nearest neighbor interpolation with a coordinate frame rotation to obtain the vertical velocity normal to the hill surface.

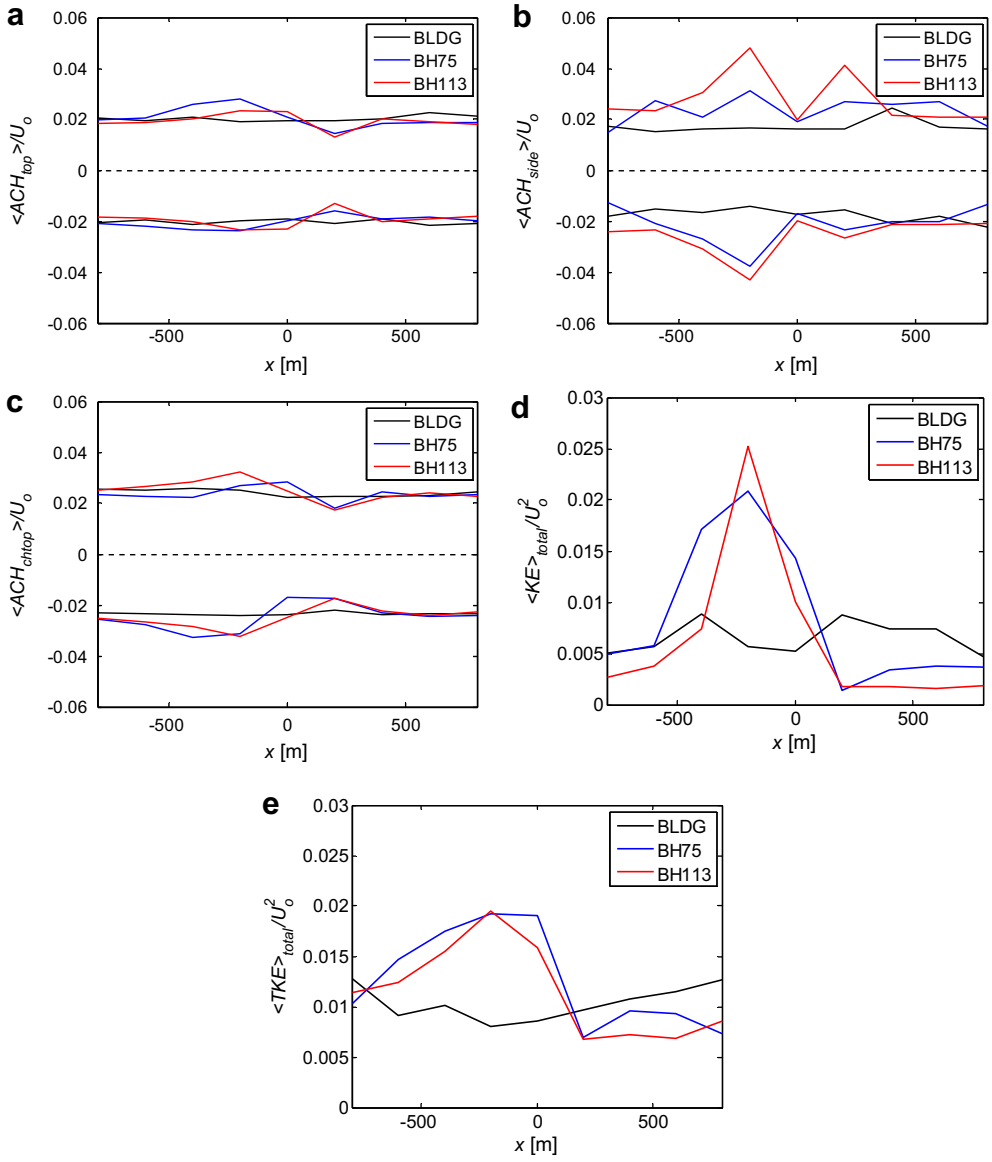

Fig. 9. Bulk air exchange rates (ACH), turbulent kinetic energy (TKE) and kinetic energy (KE) in urban canopy normalized by the free stream velocity at the top of the domain U_o. There are nine canyons at $x = -800, -600, -400, -200, 0, 200, 400, 600$ and 800 m a) $<ACH_{top}>$ through the top of the canyon; b) $<ACH_{side}>$ through the side of the canyon; c) $<ACH_{chtop}>$ through the top of the "channel" parallel to the x-axis; d) volume averaged $<KE>_{total}$; e) volume averaged $<TKE>_{total}$ (see Figs. 4 and 8).

due to horizontal homogeneity of the buildings. $<ACH_{top}>$ and $<ACH_{side}>$ are approximately equal to 0.02 for BLDG while $<ACH_{chtop}>$ is slightly larger at around 0.025. The magnitudes and trends observed in $<ACH_{top}>$ and $<ACH_{chtop}>$ for BH75 and BH113 are similar (Fig. 9a,c). A slight increase in these quantities is observed upwind of the hillcrest and a slight decrease is observed downwind of the hillcrest, and this trend is consistent with the behavior of $<KE>_{total}$ and $<TKE>_{total}$ for BH75 and BH113. A remarkable trend can be observed in $<ACH_{side}>$ (Fig. 9b) for BH75 and BH113; in both simulations $<ACH_{side}>$ increases about 200 m upwind and downwind of the hillcrest. All air exchange rates become approximately equal at $x = 0$ among the BLDG, BH75 and BH113 simulations because in the BH simulations the roofs of the adjacent building rows at the hillcrest are at the same height, so the shape of the urban canyon, and consequently the structure of the roof level shear layer, are similar in all three domains (see Fig. 10). $<KE>_{total}$ and $<TKE>_{total}$ increase dramatically around 250 m upwind of the hillcrest but decrease sharply in the lee of the hill (Fig. 9d,e).

TKE in the atmospheric surface layer is also an important determinant of turbulent mixing and dispersion. Streamwise-vertical (x–z) slices of TKE through the center of the simulation domains are shown in Fig. 10. There are patches with large TKE downwind of the hill in H75 and H113, and the TKE of H113 is larger than for H75. Considering the simulations containing buildings, the TKE distribution of BH75 and BH113 are qualitatively similar but TKE for BH113 is much larger due to the large separation region in the lee of the hill and its effect on the flow above the separation region. In BH75 and BH113 simulations the regions of largest TKE occur in the wake of the hill. In both BH simulations there is a zone of low TKE above the hillcrest. With the exception of this zone of small TKE, the TKE of BLDG is similar in magnitude to BH75 but homogeneous in the x direction. Fig. 10d,e show an increase in TKE at the leeward side of the urban canyon at the hillcrest, and at the center of the urban canyon in the space upwind of the hillcrest which is consistent with Fig. 9a,e. The TKE is lowest in the urban canyons located in the wake of the hill.

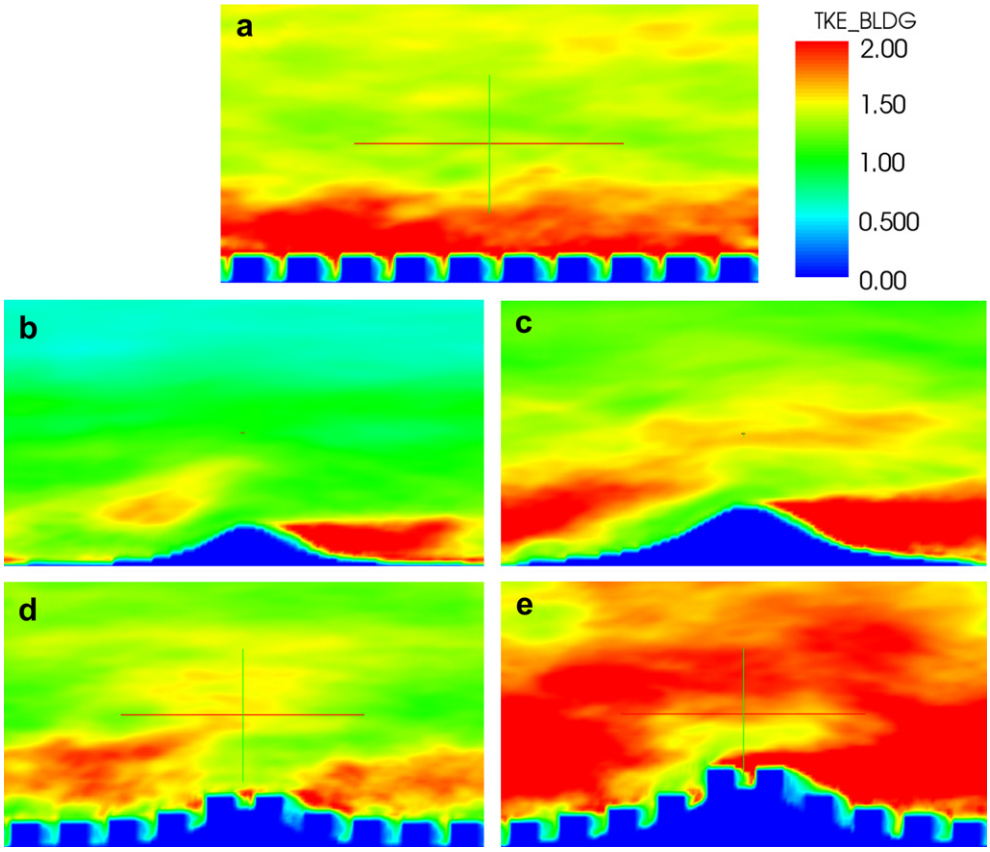

Fig. 10. x–z slices of mean resolved $\langle\overline{\mathrm{TKE}}\rangle$ m^2 s^{-2} through the center of the domain for all five simulations. The bottom half of the simulation domain is shown ($x = -1000 < x < 1000$ m, $y = 300$ m and $0 < z < 500$ m). a) BLDG, b) H75, c) H113, d) BH75, e) BH113. All figures use the same color scale.

Variances of the velocity components are critical inputs into most bulk dispersion models. For example, in Gaussian dispersion models for neutral conditions the lateral and vertical spreading of a plume is proportional to the dimensional standard deviations of the spanwise (σ_v) and vertical velocity (σ_w), respectively [42]. Fig. 11 shows profiles of σ_v, σ_w and <TKE> averaged over horizontal planes (and time). With the exception of the roughness sub-layer, the velocity variances and the TKE are larger in BH113 than in the other simulations. The maximum velocity variance usually occurs at the height of the tallest obstacle, not at the average obstacle height, which is important for the representation of urban areas in meteorological models. As expected, H113 has larger TKE and velocity variances than H75. BH75 usually has smaller TKE and velocity variances than BLDG which is surprising since roughness was added in BH75. We posit that the wake region in BH75 reduces the shear stress there resulting in less effective roughness to the flow. The same effect should occur for BH113, but the large size of the hill creates so much additional shear and turbulence that the TKE and velocity variances become larger than for BLDG.

4. Discussion

In the first application of a three-dimensional immersed boundary method to urban boundary layer flows, large-eddy simulation was performed over five different surface boundaries representing smooth hilly terrain (H75 and H113), flat urban terrain (BLDG) and hilly urban terrain (BH75 and BH113). Model validation of flow over the Witch of Agnesi hills with different heights exhibited velocity speed-up effect and separation consistent with experimental data from wind tunnel measurements.

The goal of this analysis was to determine when natural topographic variations on the order of the building height will have significant effects on the flow field, dispersion parameters and their determinants in the urban boundary layer. We simulated flow over moderately sloped hills (maximum slope of 0.26) where weak separation occurs and varied only the hill height. For flow over hills other authors have shown that the hill slope is a critical parameter which determines flow separation [38,43]. The impact of separation and changes in the onset of separation of flow over bare hills versus hills with buildings is an important topic that was beyond the scope of this study.

Natural topography with buildings (BH75 and BH113) leads to a reduction in the mean velocity in the canopy layer and surface layer compared to buildings over a flat surface (BLDG). For the urban canopy on a 75 m hill (BH75), the velocity profiles are similar to those of BLDG. Surface layer shear stress and TKE decrease for BH75 compared to the same building array on a flat surface (BLDG). Small surface layer shear stress and TKE imply reduced dispersion of air pollution above the buildings in the BH75 model relative to BLDG. This result suggests that air pollution concentrations from vehicles, domestic combustion and industrial emissions may be enhanced in cities with moderately sized hills (i.e. hill height to build height ratio of about 1). This finding is significant because smog production is already enhanced in urban areas due to elevated air temperatures caused by the urban heat island effect, and day over day accumulation of pollution from the nocturnal residual layer that becomes entrained in the mixed layer [44,45]. Smog is hazardous to human health and is transported between the surface layer and urban canyon by intermittent flow structures called cavity eddies and flushing events [46]. In BH113 shear stress

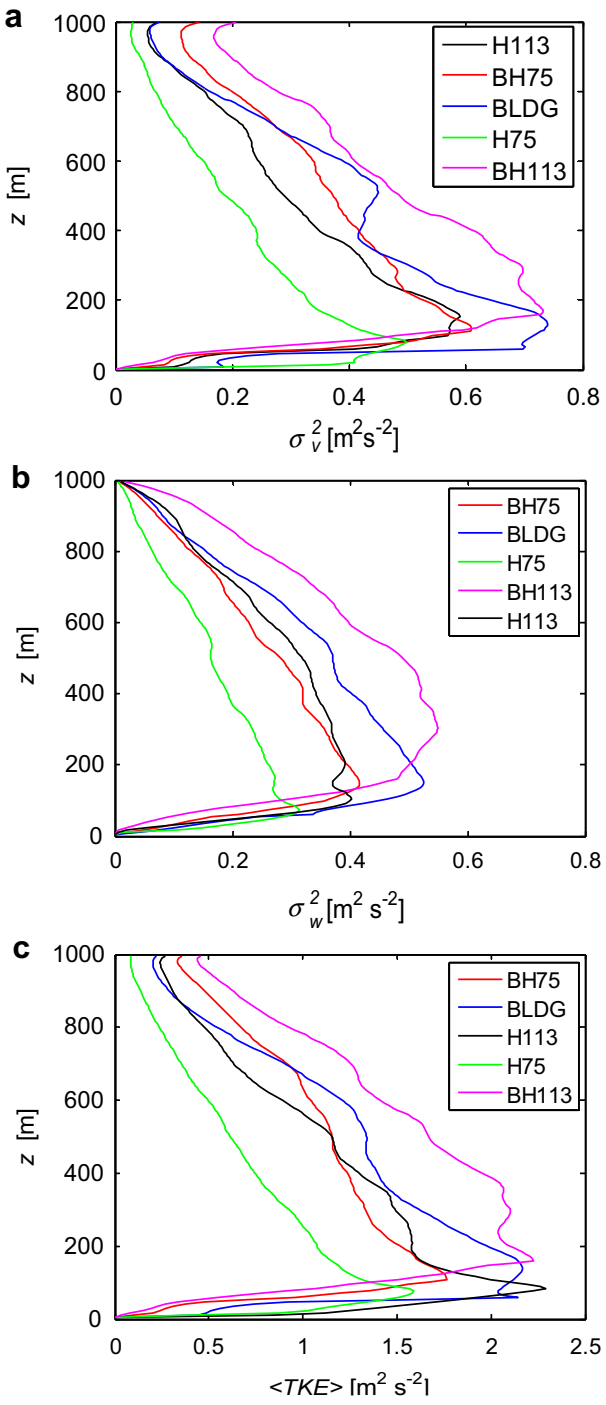

Fig. 11. Resolved a) spanwise velocity variance (σ_v), b) vertical velocity variance (σ_w) and c) TKE averaged in x and y (and time).

and TKE significantly increase which leads to enhanced dispersion and air exchange relative to BLDG and BH75. This implies that air quality may improve in cities with large hills (hill height to building height greater than 2) relative to moderate hills, although it is important to note that localized zones of poorly mixed air in urban canyons immediately downwind of the hillcrest that are not observed in flat urban areas.

Air exchange rates for the urban canyon are important to judge dilution and removal of street vehicle emissions. The bulk KE and TKE in the urban canyons for BH75 and BH113 are similar. Mixing of air in urban canyons upwind of the hillcrest in the BH simulations is dramatically enhanced relative to BLDG case, but in canyons downwind of the hill less mixing occurs. The magnitudes of $<ACH_{top}>$ and $<ACH_{chtop}>$ are similar in all three simulations, however, a slight reduction in these values for urban canyons in the lee of the hill in BH75 and BH113 suggests that those areas will experience less dilution of street level emissions when compared to other areas in the domain. A dramatic increase in $<ACH_{side}>$ occurs at a short distance upwind and downwind of the hillcrest in both BH75 and BH113. This trend is interesting when considered in the context of $<ACH_{top}>$ and $<ACH_{chtop}>$ at the same locations, because it suggests that emissions originating within the urban canopy will become well mixed at the sub-canopy level, but have a reduced tendency to become diluted with clean air from above the urban canopy. This is detrimental for human health and comfort and important for urban design, because intense mixing of pollution within the urban canopy increases the likelihood that a large number of people will be adversely affected by air pollution. It also suggests that air pollution from large thoroughfares can spread laterally into surrounding neighborhoods.

The magnitude of bulk air exchange rates in all of our simulations were similar to the results obtained from the numerical simulations of Liu et al. (2005). In the BH75 and BH113 simulations street canyons upwind of the hillcrest are ventilated through both the top and sides of the urban canyon, at the hillcrest ventilation occurs approximately equally through the top and side of the canyon and in the lee of the hill ventilation is primarily through the side of the canyon. These findings suggest that the layout of streets and buildings in hilly cities is especially important to maximize canopy ventilation. Building layout in urban areas built on complex terrain should be carefully planned and evaluated (with the aid of CFD simulations) to assess canopy ventilation effects prior to new urban development and/or modification of structures in an existing urban area.

5. Conclusions

Terrain undulations are a significant factor in the dynamics of the urban boundary layer and urban dispersion, even for moderate terrain slope ratio (0.26) and small hill to building height ratio (1.5 for BH75). This result was expected for large hill to building height ratio; however, we have shown the remarkable result that hills with relatively moderate height (hill height on the order of the building height) strongly modify the in-canyon mixing behavior and canyon-atmosphere exchange. Atmospheric boundary layer dispersion properties are affected non-linearly with small hills slightly reducing velocity variances while large hills strongly increase same. Results from experiments or simulations that investigate buildings on a flat terrain are not directly applicable to urban areas with even modest hills. Large population centers are frequently located in coastal urban areas (e.g. San Francisco, Barcelona, Tokyo, Brisbane), and in many coastal cities hilly terrain with typical height variations on the order of or larger than the building height is common. Future efforts in urban dispersion research should focus on evaluating critical hill heights or slopes for different urban substrates for which departures from horizontal cases warrant a case-by-case examination.

Acknowledgments

The authors thank Anthony Dominguez (UCSD) for his helpful comments and suggestions on an early draft of this manuscript. Funding for this research was provided by an NSF CBET CAREER award.

Appendix A

Maria Gaetana Agnesi was an 18th century Italian mathematician and professor at the University of Bologna. In the course of writing this manuscript we came across a rather amusing story that explains how the famous curve known as the Witch of Agnesi (Eq. (6)) earned its peculiar title. Agnesi studied the curve and described its shape by the Italian word *aversiera*, meaning "to turn". Agnesi documented her work in a teaching manual that was later obtained by Cambridge mathematician John Colson. Colson, whose native language was English, apparently confused the word *aversiera* with *aversiere* which means "witch" or "wife of the devil" and the name stuck henceforward. Many years later British astronomer and author David Darling observed with amusement that the shape of Eq. (6) actually resembles a witch's hat [47].

References

[1] Hanna SR, Tehranian S, Carissimo B, Macdonald RW, Lohner R. Comparisons of model simulations with observations of mean flow and turbulence within simple obstacle arrays. Atmos Environ 2002;36:5067–79.
[2] Tseng YH, Meneveau C, Parlange MB. Modeling flow around bluff bodies and predicting urban dispersion using large eddy simulation. Environ Sci Technol 2006;40:2653–62.
[3] Xie ZT, Coceal O, Castro IP. Large-eddy simulation of flows over random urban-like obstacles. Boundary-Layer Meteorol 2008;129:1–23.
[4] Kanda M, Moriwaki R, Kasamatsu F. Large-Eddy simulation of turbulent organized structures within and above explicitly resolved cube arrays. Boundary-Layer Meteorol 2004;112:343–68.
[5] Coceal O, Thomas TG, Castro IP, Belcher SE. Mean flow and turbulence statistics over groups of urban-like cubical obstacles. Boundary-Layer Meteorol 2006;121:491–519.
[6] Li XX, Liu CH, Leung DYC. Large-eddy simulation of flow and pollutant dispersion in high-aspect-ratio urban street canyons with wall model. Boundary-Layer Meteorol 2008;129:249–68.
[7] Liu CH, Leung DYC, Barth MC. On the prediction of air and pollutant exchange rates in street canyons of different aspect ratios using large-eddy simulation. Atmos Environ 2005;39:1567–74.
[8] Kaimal JC, Finnigan JJ. Atmospheric boundary layer flows: their structure and measurement. New York: Oxford University Press; 1994.
[9] Jackson PS, Hunt JCR. Turbulent wind flow over a low hill. Q J Roy Meteorol Soc 1975;101:929–55.
[10] Britter RE, Hunt JCR, Richards KJ. Airflow over a two-dimensional hill: studies of velocity speed-up, roughness effects and turbulence. Q J Roy Meteorol Soc 1981;107:91–110.
[11] Belcher SE, Hunt JCR. Turbulent flow over hills and waves. Annu Rev Fluid Mech 1998;30:507–38.
[12] Poggi D, Katul GG. Turbulent flows inside forested hilly terrain: the recirculation region. Q J Roy Meteorol Soc 2007;133:1027–39.
[13] Poggi D, Katul GG, Finnigan JJ, Belcher SE. Analytical models for the mean flow inside dense canopies on gentle hilly terrain. Q J Roy Meteorol Soc 2008;134:1095–112.
[14] Finnigan JJ, Belcher S. Flow over a hill covered with a plant canopy. Q J Roy Meteorol Soc 2004;130:1–29.
[15] Ross AN, Vosper SB. Neutral turbulent flow over forested hills. Q J Roy Meteorol Soc 2005;131:1841–62.
[16] Finnigan JJ, Brunet Y. Turbulent airflow in forests on flat and hilly terrain. In: Coutts MP, Grace J, editors. Wind and trees. New York: Cambridge University Press; 1995. p. 3–40.
[17] Brown AR, Hobson JM, Wood N. Large-eddy simulation of neutral flow over rough sinusoidal ridges. Boundary-Layer Meteorol 2001;98:411–41.
[18] Pope SB. Turbulent flows. New York: Cambridge University Press; 2000.
[19] Deardorff JW. A numerical study of three-dimensional turbulent channel flow at large Reynolds numbers. J Fluid Mech 1970;41:453–80.
[20] Moeng CH. A large-eddy simulation model for the study of planetary boundary-layer turbulence. J Atmos Sci 1984;46:2311–30.
[21] Mason P. Large-eddy simulation: a critical review of the technique. Q J Roy Meteorol Soc 1994;120:1–26.
[22] Albertson JD, Parlange MB. Natural integration of scalar fluxes from complex terrain. Adv Water Resour 1999;23:239–52.
[23] Bou-Zeid E, Meneveau C, Parlange MB. A scale-dependent Lagrangian dynamic model for large-eddy simulation of complex turbulent flows. Phys Fluids 2005;17:025105.
[24] Kanda M. Progress in urban meteorology: a review. J Meteorological Soc Jpn 2007;85B:363–83.
[25] Orszag SA, Pao Y, Metcalfe RW. Numerical computation of turbulent shear flows. Bull Am Phys Soc 1976;18(11):1488.
[26] Peskin CS. Flow patterns around heart valves: numerical method. J Comput Phys 1972;10:252–71.
[27] Mohd-Yusof J. Combined immersed boundary/B-spline methods for simulations of flows in complex geometries. In: Annual research briefs. Stanford, CA: NASA Ames Research Center/Stanford University Center for Turbulence Research; 1997. p. 317–27.
[28] Tseng YH, Ferziger JH. A ghost-cell immersed boundary method for flow in complex geometry. J Comput Phys 2003;192:593–623.
[29] Mahrer Y. An improved numerical approximation of the horizontal gradients in a terrain-following coordinate system. Mon Weather Rev 1984;112:918–22.
[30] Lundquist KA, Chow FK, Lundquist JK. An immersed boundary method for the weather research and forecasting model. Mon Weather Rev 2010;138:796–817.
[31] Wan F, Porté-Agel F, Stoll R. Evaluation of dynamic subgrid-scale models in large-eddy simulations of neutral turbulent flow over a two-dimensional sinusoidal hill. Atmos Environ 2007;41(13):2719–28.
[32] Meneveau C, Katz J. Scale-invariance and turbulence models for large-eddy simulation. Annu Rev Fluid Mech 2002;32:1–32.
[33] Kleissl J, Parlange MB, Meneveau C. Field experimental study of dynamic Smagorinsky models in the atmospheric surface layer. J Atmos Sci 2004;61:2296–307.
[34] Smagorinsky J. General circulation experiments with the primitive equations: I. The basic experiment. Mon Weather Rev 1963;91:99–164.
[35] Lilly DK. The representation of small-scale turbulence in numerical simulation experiments. Proceedings of the IBM scientific computing symposium on environmental sciences. New York: Yorktown Heights; 1967. p. 195.
[36] Meneveau C, Lund T, Cabot WA. Lagrangian dynamic subgrid-scale model of turbulence. J Fluid Mech 1996;319:353–85.
[37] Porté-Agel F, Meneveau C, Parlange MB. A scale-dependent dynamic model for large-eddy simulation: application to a neutral atmospheric boundary layer. J Fluid Mech 2000;415:261–84.
[38] Gong W, Taylor PA, Doernbrack A. Turbulent boundary layer flow over fixed aerodynamically rough two-dimensional sinusoidal waves. J Fluid Mech 1996;312:1–37.
[39] Clark TA. small-scale dynamic model using a terrain-following coordinate transformation. J Comput Phys 1977;24:186–215.
[40] Bou-Zeid E, Overney J, Benedict DR, Parlange MB. The effects of building representation and clustering in large eddy simulations of flows in urban canopies. Boundary-Layer Meteorol 2009;132(3):1472–573.
[41] Franke J, Hellsten A, Schlunzen H, Carissimo B. Best practice guideline for the CFD simulation of flows in the urban environment (COST Action 732), http://www.mi.uni-hamburg.de/fileadmin/files/forschung/techmet/cost/cost_732/pdf/BestPractiseGuideline_1-5-2007-www.pdf; 1 May, 2007. Accessed 22 June, 2011.
[42] Taylor GI. Diffusion by continuous movements. Proc London Math Soc 1922;20:196–212.
[43] Kuzan JD, Hanratty TJ, Adrian RJ. Turbulent flows with incipient separation over solid waves. Exps Fluids 1989;7:88–98.
[44] Jacob DJ, Logan JA, Gardner GM, Yevich RM, Spivarkovsky CM, Wofsy S, et al. Factors regulating ozone over the United States and its export to the global atmosphere. J Geophys Res 1993;98:14817–26.
[45] Stull RB. An introduction to boundary layer meteorology. The Netherlands: Kluwer Academic Publishers; 1988.
[46] Takimoto H, Sato A, Barlow J, Moriwaki R, Inagaki A, Onomura S, et al. Particle image velocimetry measurements of turbulent flow within outdoor and indoor scale models and flushing motions in urban canopy layers. Boundary-Layer Meteorol 2011;140(2):295–314.
[47] Darling D. The universal book of mathematics: from abracadabra to Zeno's paradoxes. New Jersey: John Wiley & Sons; 2004.